3-16-2018

Forecasting the Eruption of an Open-Vent Volcano Using Resonant Infrasound Tones

Jeffrey B. Johnson
Boise State University

Leighton M. Watson
Stanford University

Jose L. Palma
University of Concepción

Eric M. Dunham
Stanford University

Jacob F. Anderson
Boise State University

AGU PUBLICATIONS

Geophysical Research Letters

RESEARCH LETTER
10.1002/2017GL076506

Key Points:
- Volcanoes produce infrasound that is critically modulated by crater/conduit geometry
- Changes in infrasound quality and frequency are used to track the stage of a lava lake at Villarrica prior to a paroxysmal eruption
- Lessons learned suggest that infrasound should be used to monitor and forecast eruptions at open-vent volcanic systems

Supporting Information:
- Supporting Information S1
- Movie S1

Correspondence to:
J. B. Johnson,
jeffreybjohnson@boisestate.edu

Citation:
Johnson, J. B., Watson, L. M., Palma, J. L., Dunham, E. M., & Anderson, J. F. (2018). Forecasting the eruption of an open-vent volcano using resonant infrasound tones. *Geophysical Research Letters*, *45*, 2213–2220. https://doi.org/10.1002/2017GL076506

Received 22 NOV 2017
Accepted 5 FEB 2018
Accepted article online 12 FEB 2018
Published online 8 MAR 2018

Forecasting the Eruption of an Open-Vent Volcano Using Resonant Infrasound Tones

Jeffrey B. Johnson[1], Leighton M. Watson[2], Jose L. Palma[3], Eric M. Dunham[2,4], and Jacob F. Anderson[1]

[1]Department of Geosciences, Boise State University, Boise, ID, USA, [2]Department of Geophysics, Stanford University, Stanford, CA, USA, [3]Departamento Ciencias de la Tierra, University of Concepción, Concepción, Chile, [4]Institute for Computational and Mathematical Engineering, Stanford University, Stanford, CA, USA

Abstract Open-vent volcanic systems with active degassing are particularly effective at producing infrasound that exhibits resonant tones controlled by the geometry of the volcano's crater. Changes in the infrasound character can thus provide constraints on a crater's lava level, which may vary dynamically in the lead-up to an eruption. Here we show that the increasing frequency content and damping characteristics of the resonant infrasound at Volcán Villarrica (Chile) relate to lava lake position in its crater/conduit preceding its 2015 eruption. We model the acoustic response of Villarrica's crater to determine that the lake began to rise on 27 February and reached the flared upper part of Villarrica's crater before oscillating during the two days prior to the 3 March paroxysm and 1.5 km-high lava fountain. This study demonstrates the utility of remote infrasound monitoring for future eruptions of Villarrica and other analogous open-vent volcanoes.

Plain Language Summary Volcanic craters are like giant musical instruments in the sense that the sounds that volcanoes produce can change as the crater size evolves. We track the changing tones and resonance of low-frequency infrasounds at Volcan Villarrica (Chile) and attribute their variations as a response to the rise of the lava lake in the crater. We use infrasound data and employ numerical models to track the depth of the lava lake over time. Significant changes in infrasound character occurred just prior to a violent 3 March 2015 eruption leading us to propose that monitoring volcano infrasound resonance is important for forecasting future volcanic eruptions.

1. Introduction

A primary goal of volcanology is to identify eruption precursors in order to better forecast and mitigate the impacts of eruptions. Volcano monitoring makes use of continuous infrasound measurements (sound below 20 Hz) for understanding the dynamics of eruptions ranging from small to large (Fee & Matoza, 2013) and for a wide range of mechanisms, including explosions (Johnson & Miller, 2014; Morrissey & Chouet, 1997), gas jetting (Matoza et al., 2013), and surface mass movements like pyroclastic flows and lahars (Johnson & Palma, 2015; Yamasato, 1997). Infrasound studies have proven useful in remotely quantifying eruption parameters (Fee et al., 2017; Woulff & McGetchin, 1976); however, until present, there has been limited application and understanding of how to use infrasound to identify eruption precursors.

Actively degassing open-vent volcanoes, such as Kilauea (Hawaii) and Villarrica (Chile), are energetic, continuous, and efficient sources of infrasound (Johnson & Ripepe, 2011). Continuous or discrete bursts of degassing from the crater floor or lava lake surface excite acoustic waves through resonance of the air mass within the crater. Because the infrasound signal is influenced by the geometry of the crater, several studies have utilized resonant infrasound observations to infer crater dimensions and lava lake depth (Fee et al., 2010; Goto & Johnson, 2011; Lyons et al., 2016; Richardson et al., 2014; Spina et al., 2014). This study demonstrates how changing infrasound character from Volcán Villarrica (Chile) can be used to track lava level at open vent volcanoes in the lead-up to a violent paroxysm. Tracking the level of the lava-free surface may otherwise be challenging using other types of monitoring techniques.

2. Volcán Villarrica and Its 2015 Paroxysm

Volcán Villarrica (Chile) is an ~2,950 m tall stratovolcano hosting a long-lived convecting lava lake at the bottom of a steep-walled, summit crater. Its location is only 17 km from the municipality of Pucon,

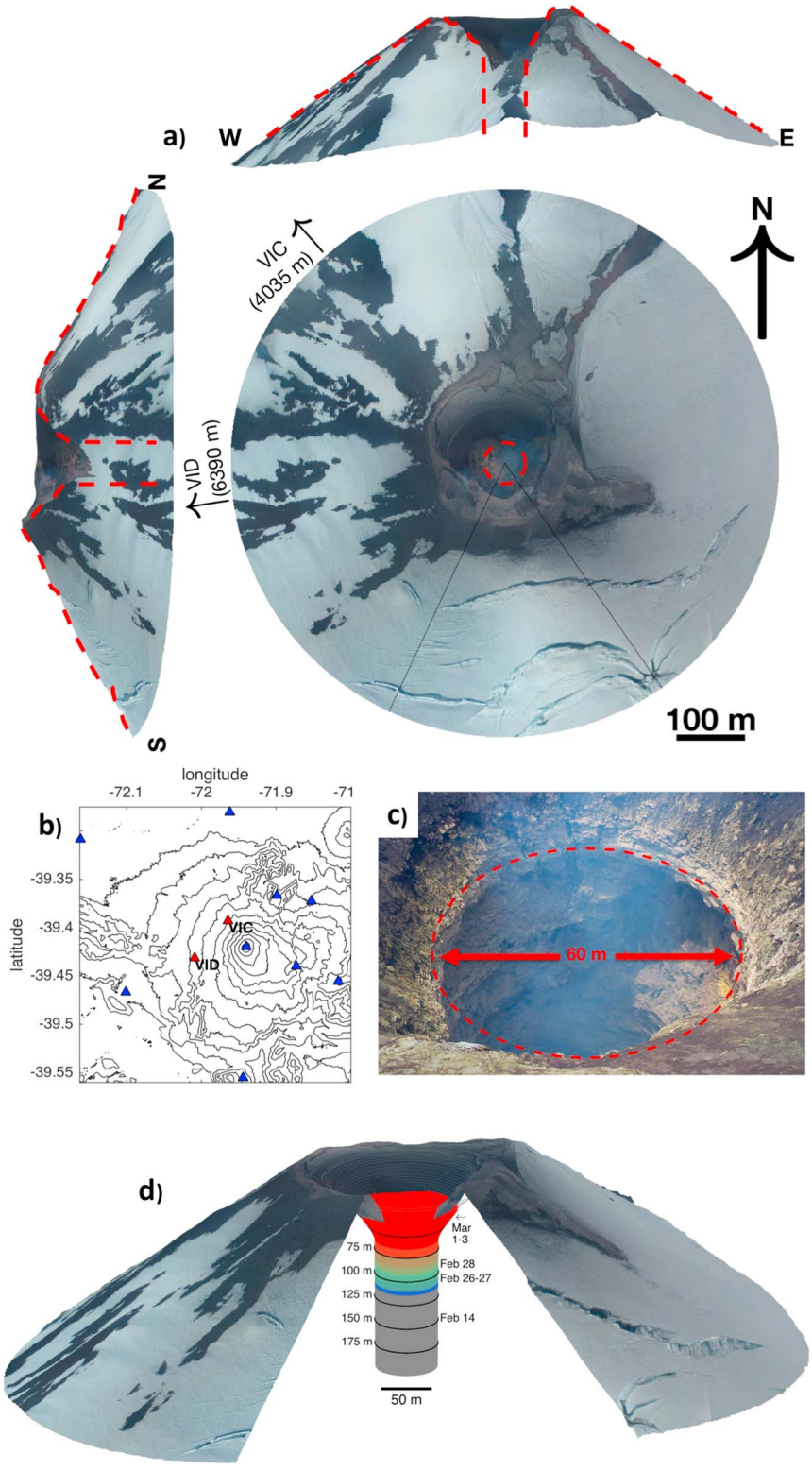

Figure 1. Villarrica's crater geometry. (a) Plan and profile views of Villarrica's upper edifice derived from structure from motion (SfM) for a 14 February 2015 overflight. Distance and direction to infrasound stations are indicated. (b) Map of 2015 infrasound network deployment including the two stations, VIC and VID, used in this study. (c) Photo taken from crater rim in 2011 showing an ~30 m radius vertical-walled shaft extending down to an out-of-sight lava lake. (d) Oblique-view, cut-away orthomosaic of volcano showing progressive ascent of lake levels as described in this paper. An animation of the time progression of the lava level and its associated infrasound are provided as supporting information.

whose permanent population of 25,000 swells by an order of magnitude during the austral summer tourist season. Pucon is particularly exposed to volcano hazards because mountain topography and Lake Villarrica restrict evacuation routes. Volcano monitoring, supported by a telemetered seismic and geodetic network and real-time camera surveillance, is primarily maintained by the Chilean volcano monitoring authority (Volcano Observatory of the Southern Andes [OVDAS]/Servicio Nacional de Geología y Minería [SERNAGEOMIN]).

Villarrica is a classic open-vent volcano that degasses continuously and produces both tremor and discrete explosion infrasound, which display pronounced resonant tones peaked around 1 Hz (Goto & Johnson, 2011; Johnson et al., 2012, 2004; Richardson et al., 2014; Ripepe et al., 2010). A magma column with a 20–40 m radius is generally exposed as a lava lake at the crater bottom, and the lake's vigorous degassing is thought to be responsible for the excitation of infrasound. Although glow from the lava lake is often visible at night from as far away as Pucon, its surface is most often out of view from the summit due to the flaring crater geometry that slopes downward from the rim for about 60–80 m and then continues as a vertical-walled shaft (Goto & Johnson, 2011; Moussallam et al., 2016; Palma et al., 2008) (Figure 1). Previous work using seismic and acoustic measurements has shown that the level of the lava lake fluctuates over monthly time scales (Richardson et al., 2014). These inferences are supported by visual observations from mountain guides who regularly visit the summit (pers. comm. Pucon Mountain Guides; www.povi.cl) and report that activity is normally manifested by roiling of the lava lake surface, which feeds small strombolian eruptions typically confined to the interior of the crater. This style of activity has been the norm at Villarrica since the last major eruption in 1984–1985 when the lava lake previously overtopped the crater rim.

A 30 year period of quiescence at Villarrica ended at 3 a.m. local time (6 a.m. universal time coordinated) on 3 March 2015 when the volcano erupted in a short-duration (~30 min) violent paroxysm. The eruption produced a 1.5 km-high lava fountain and was quantified as Volcano Explosivity Index 2 (10^6–10^7 m^3 of erupted tephra; Newhall & Self, 1982). The eruption was preceded by elevated seismic activity reported by OVDAS/SERNAGEOMIN, which led to restricted summit access beginning on 7 February. The alert level was further elevated to "yellow" in the early morning of 1 March in response to observations of frequent nighttime strombolian explosions expelling ballistics well beyond the crater rim. Further increase in the intensity of strombolian activity prompted an "orange" alert on 2 March, a timely warning by OVDAS/SERNAGEOMIN that preceded the paroxysmal eruption by about half a day. During the monthlong lead-up to the 3 March eruption, occasional visual observations (afforded by OVDAS/SERNAGEOMIN overflights) hinted at fluctuating levels of the lava lake (Figure 2).

3. Infrasound Data

The lead-up to the 3 March eruption was well recorded by our nontelemetered infrasound monitoring network of ten 3-element, 30 m aperture arrays deployed at distances of 4 to 22 km from the summit (Figure 1b). The network was deployed in January 2015 and complemented an infrasound station maintained by the University of Concepcion since 2014. Although the eruption destroyed two of our summit infrasound stations, the other stations remained operational through the duration of the crisis and into the spring of 2015 as the volcano returned to its normal mode of activity.

Infrasound data were collected from the network of arrays, which were situated with a broad distribution of azimuths relative to the summit. We present data here from the two infrasound stations closest to the summit (Figure 1a) because their recordings appear least affected by atmospheric propagation effects. Station VIC (4.0 km to the NW of the vent), operational between 9 January through 10 June, represents the longest continuous record; however, station VID (6.4 to the W of the vent) possessed the best signal-to-noise during the week preceding the 3 March eruption and is used in the explosion waveform analysis. Infrasound data were continuously recorded using 24-bit loggers at 100 Hz and identical MEMS-based transducers (Marcillo et al., 2012), which possessed a flat frequency response between 0.04 Hz and a 50 Hz Nyquist frequency. The sensors possessed a linear dynamic range of ±125 Pa.

The preeruption month-long infrasound chronology indicates variations in radiated acoustic power, which is possibly related to fluctuations in the intensity of degassing (Figure 2a). Hourly acoustic power mimicked seismic observations reported by OVDAS/SERNAGEOMIN, which indicated modest increases in seismic radiation as early as 13 January and more significant increases on 4 February with a peak on 6 February. Both

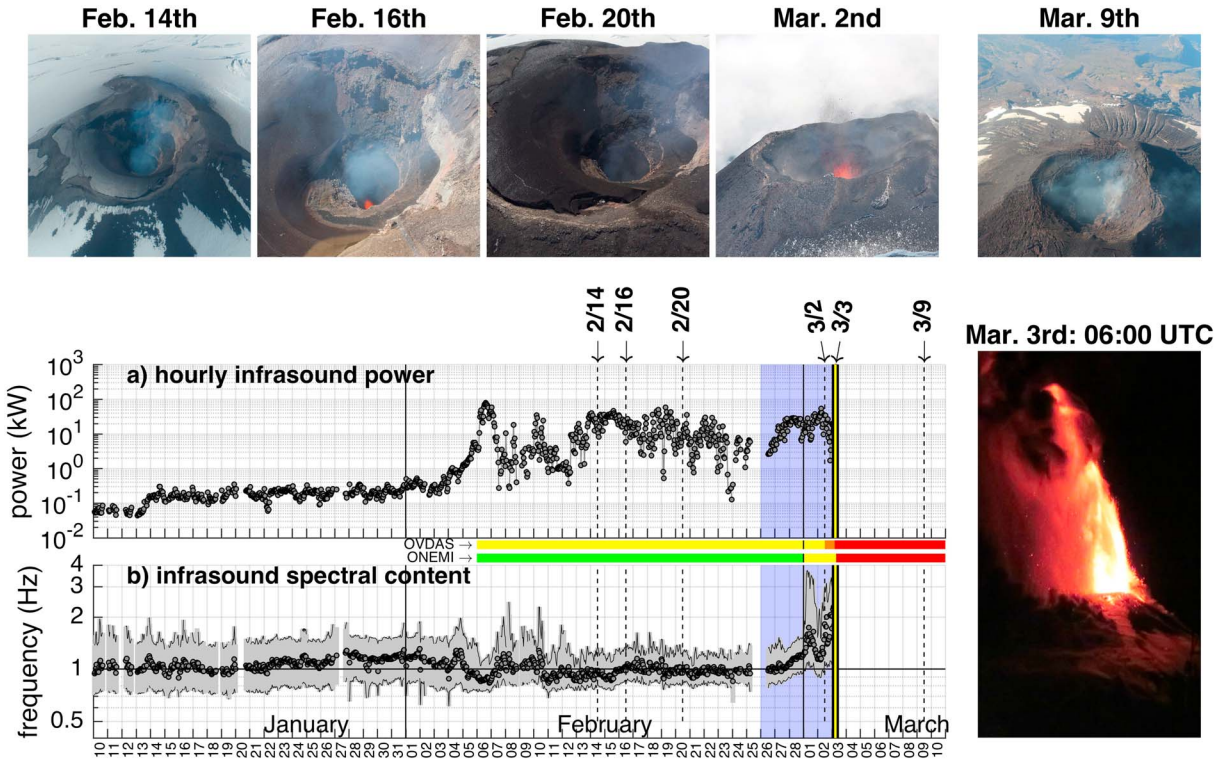

Figure 2. Infrasound chronology. Two-month infrasound record from VIC showing (a) hourly acoustic power (calculated assuming isotropic radiation) and (b) infrasound spectral content recorded at station VIC, 4 km northwest of the summit. Spectral content is indicated for 25th and 75th cumulative power (gray shading) and 50th percentile cumulative power (circles) for 0.5–10 Hz band-limited infrasound. Data gaps are periods of relatively poor signal coherency across the VIC array attributed to wind noise. Timing is indicated for the government agency alerts and aerial-view photographs.

infrasound and seismic power varied throughout February; however, no systematic increases were observed leading up to the 3 March eruption. It was not until the last hours of February that the spectral content of the continuous infrasound departed significantly from its long-term character (Figure 2b). This change occurred several days before the paroxysm, and its relevance as an important precursor was not recognized until now.

In this study, we focus on the week-long record of infrasound leading up to the paroxysm (Figures 2 and 3). Continuous infrasonic tremor was not evident during this period; however, high-amplitude (10^0–10^1 Pa at 4 km) explosion signals were common, occurring at a rate of a few thousands per day. These explosion signals were windowed from beam-stacked time series filtered above 0.5 Hz to remove contamination from microbaroms. Characteristic hourly explosion waveforms are then taken as the stack of the 40 highest amplitude signals recorded during a particular hour and are aligned according to their optimal cross-correlation time lags (Figure 3).

The stacked waveforms are characterized by an impulsive compressional pulse, typical of discrete Strombolian explosions (e.g., Johnson et al., 2004), followed by a rarefaction and a gradually decaying sinusoidal coda (Figure 3c). In the frequency domain, the signals are monotonic (or monochromatic) with a clear fundamental peak frequency f_p and lack of pronounced integer overtones (Figure 3f). Between 27 February and the paroxysmal eruption on 3 March the characteristic explosion waveform shape evolved from gradual coda decay (Figure 3a) to nonexistent coda (Figure 3b) indicating an increase in the amount of damping in the crater source, quantified by a decrease in the quality factor Q. Quality factor in the frequency domain is evident as a broadening of the resonant peak (Figures 3d and 3e) and can be calculated as peak frequency f_p divided by the spectral bandwidth ($\Delta Q = f_p/\Delta f$), where bandwidth corner frequencies are found at one half of the peak frequency's power. The associated exponential decay constant, $\alpha = \pi\Delta f = \pi f_p/Q$ (Rossing & Fletcher, 2004), is inversely proportional to quality factor and is used to verify an appropriate envelope for the time series coda oscillations (e.g., Figures 3a and 3b).

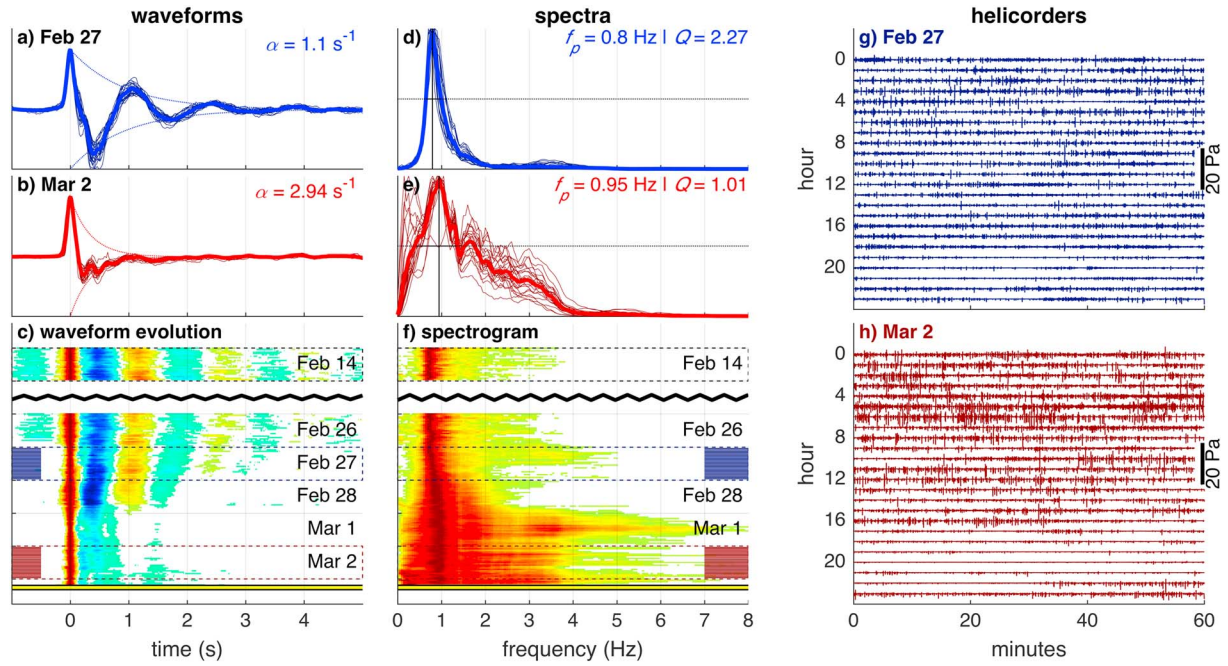

Figure 3. Explosion signals and spectra. (a and b) Characteristic lava lake explosion waveforms are indicated for 27 February and 2 March and show hourly averaged (thin lines) and daily averaged (thick lines) for 1,000 events (i.e., ~40 per hour). (c) Time evolution of hourly event stacks is displayed with color representing normalized amplitudes. (d and e) Normalized power spectra for the time series presented in (a) and (b). Exponential decay time constants (α) are calculated from spectral Q and f_p. (f) Spectogram shows evolution in frequency content. Displayed infrasound was recorded at VID, 6.4 km west of the summit. (g and h) Helicorder-style infrasound records from 27 February and 2 March recorded at VID.

4. Infrasound Modeling

We hypothesize that the observed decrease in infrasound quality factor, associated with a general increase in resonant frequency (Figure 4), is due primarily to the ascent of the lava lake prior to the 3 March eruption. The resonant frequency increases because as the lava lake rises, the effective length of the acoustic resonator shortens. The quality factor, which is inversely proportional to the damping in the system, is also dependent upon the length of the acoustic resonator and its shape. Energy loss, independent of factors such turbulent dissipation or wall friction, occurs principally through acoustic radiation, which is controlled by the impedance contrast between the crater and the atmosphere. An acoustic resonator with a high-quality factor is able to efficiently trap acoustic energy and only radiate at the resonant frequency, such as for the case of a long narrow pipe or when the lava lake is deep and in the shaft section of Villarrica's crater. Conversely, an acoustic resonator with a low-quality factor is able to efficiently radiate energy into the atmosphere. An example of a low Q system is a flared horn with a broad opening such that the outlet impedance of the horn is closely matched to the acoustic impedance of the atmosphere (Rossing & Fletcher, 2004).

We model the evolution of both f_p and Q as a function of the lava lake level, which is allowed to rise and fall within a constrained crater geometry. We model the crater's shape as an axisymmetric approximation that is derived from structure from motion (SfM). Imagery for SfM was obtained during an over-flight on 14 February 2015 during which more than a thousand 12-megapixel images were acquired from ~500 m above the summit and with a cumulative 1 km field of view. An orthomosaic image and digital elevation model were generated at 1 m resolution using surveyed control points for registration and Agisoft's PhotoScan Pro Software (Figure 1). The shape of the crater down to more than 100 m below the rim was visible—and well reconstructed—but below this, a vertical shaft with 30 m radius was assumed. This crater shape is in good agreement with the 3-D morphology of Villarrica's posteruption crater from January 2016 when we revisited and obtained another SfM model.

Our numerical model, which is described in the supporting information (Carpenter et al., 1994; Karlstrom & Dunham, 2016; Lighthill, 1978; Olson, 1957; Svard & Nordstrom, 2014), calculates a spectral response

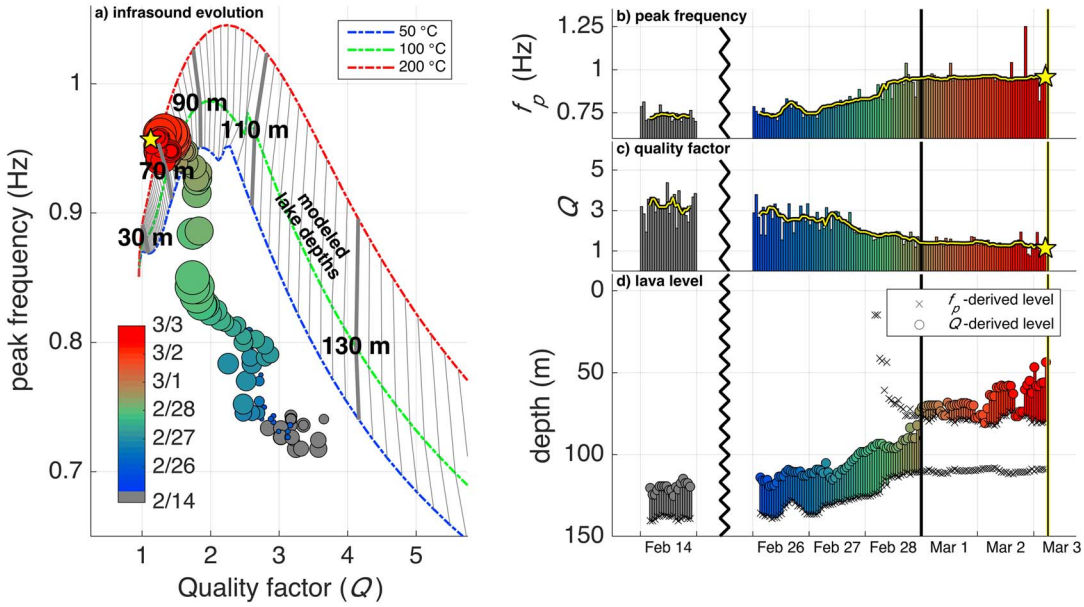

Figure 4. Evolution of resonance parameters and model results. (a–c) Variations of f_p and Q leading up to the paroxysm on 3 March (yellow stars). The yellow lines in (b) and (c) indicate 6 h running average of these spectral parameters. The data circles in (a) correspond to 6 h parameter running averages where the symbol sizes are proportional to the average explosion amplitude. Modeled f_p and Q values are shown as a function of depth and are indicated for composite crater profile and for three different conduit temperatures as described in the supporting information. (d) Evolution of inferred lava lake depths is shown for T_c = 100 °C and σ = 0.13 s. Of note, the Q-inferred lake depths are systematically shallower than frequency-derived values.

function for arbitrary axisymmetric crater geometries that can be used to extract frequency modes and spectral bandwidths. The program is written in MATLAB and is efficient, allowing quick variation of model parameters and rapid computation on a personal computer. It is complementary to 3-D finite difference time domain models, such as that of Kim and Lees (2014), which can incorporate 2-D topography to calculate infrasound synthetics but require significantly more computational power and processing time.

In this analysis, Villarrica's acoustic response functions are calculated repeatedly for varying profiles and for lava lake levels ranging from 10 m below the crater rim down to more than 200 m. For each lava lake level we determine a spectral transfer function relating the gas flux at the crater floor (i.e., at the lava lake surface) to the pressure radiated to our infrasound stations. The equivalent time domain impulse response gives the theoretical infrasound pressure wave resulting from an instantaneous explosion, or delta function outflux, at the lava lake surface. These transfer functions may then be convolved with source time functions of finite duration to synthesize realistic pressure transients and their synthetic f_p and Q values. In our modeling we use a Gaussian pulse with standard deviation of 0.13 s as a volume flux source time function. This source is equivalent to a short-duration explosion of compressed gas, and its shape well approximates the time scale of the low-Q bipolar pressure transients recorded on 2 March. This is the period when the lava lake is presumed to be high, the coda is least pronounced, and the crater acoustic response functions are least distorted.

Lava level inferences derived using resonant frequency and quality factor are generally consistent (Figure 4d). For example, when the lava lake level is below the conduit flare the depth inverted from both parameters agrees to within a few tens of meters and indicates the same relative changes. Above the flare, the resonant frequency information provides nonunique depths; that is, peak frequency is at maximum when lava is at the level of the conduit flare and decreases for both shallower and deeper lava lake levels (Figure 4a). The relationship between Q and lava lake depth, however, remains monotonic as the lava lake shallows and thus provides unambiguous estimates on the relative position of the lava lake.

Villarrica's lava lake chronology, derived from infrasound, indicates a stable, deep, and relatively typical position on 14 February some 120–130 m below the crater rim (Figures 1c and 4d). Although the lake appears to rise slightly during the last few days of February, starting on the evening of 28 February, the decreasing Q

indicates a rapid rise with the lava lake reaching 70 m, near the base of the flare, by 1 March. Varying infrasound character on 1 and 2 March suggests that the level of the lake oscillated considerably in the two days before the main eruption. This may have reflected extreme instability of the gas-charged magma conduit that culminated in the paroxysmal eruption in the early hours of 3 March.

Inferred lava lake levels responsible for the observed resonant frequencies are generally shallower than those modeled using a Bessel Horn geometry for comparable resonant frequencies in 2010 (Richardson et al., 2014). We contend that we are able to obtain good accuracy in the inferred depth history due to the improved precision of the crater profile availed by photogrammetric reconstruction and coupled use of a numerical model that can accommodate an arbitrary profile shape as well as quality factor information. Significantly, this is the first volcano infrasound study to jointly use quality factor and frequency information to calculate the depth of a lava lake. Given that Q provides nonunique depth constraints we argue for its incorporation in future studies.

5. Conclusions: On the Utility of Resonant Infrasound Monitoring

This study demonstrates that remote infrasound observations made at a safe distance from Villarrica's vent are able to provide a continuous estimate of lava lake stage. While other studies have highlighted long-term (months-long) processes leading up to the 3 March eruption (e.g., Aiuppa et al., 2017), infrasound affords an especially high-resolution (subhourly) tracking of unrest. The infrasound-derived lake levels at Villarrica are consistent with the sporadic observation of the crater lake level seen during overflight observations. Infrasound provides constraints, which are particularly vital when conditions evolve rapidly and when view to the vent is impossible.

At Villarrica, eruptions similar to, or larger than, the 3 March 2015 eruption occur every few decades (Van Daele et al., 2014) and present significant hazard to nearby urban areas and tourist interests. The relatively small 2015 eruption caused destruction of property, forced evacuations, and ravaged the mountain's tourism industry. Recognizing and interpreting Villarrica's next period of unrest are thus vital for hazard mitigation and minimizing the economic impacts. Generally, Villarrica's infrasound character and correlation with rapid magma column rise suggests that infrasound monitoring should be considered as a tool for forecasting paroxysmal eruptions at other open vent volcanoes, including systems where spectral and quality factor changes have previously been noted (e.g., Etna [Italy]; Spina et al., 2014). We envision that resonant mode infrasound monitoring could be effectively used for anticipating future eruptions at both Villarrica and other basaltic volcano analogs, including Kilauea (Hawaii), Shishaldin (Alaska), Nyiragongo (Democratic Republic of Congo), Piton de la Fournaise (Reunion), Masaya (Nicaragua), Etna and Stromboli (Italy), and Ambrym and Yasur (Vanuatu).

Acknowledgments
This collaborative work was made possible through the Fulbright Scholar's Program, National Science Foundation EAR grant 0838562 and FONDECYT grant 11121335. We appreciate helpful discussions, data, and images provided by Luis Franco and Carlos Cardoña of OVDAS/SERNAGEOMIN. Aerial imagery on 14 February used for SfM reconstruction was collected in collaboration with Werner Keller (www.povi.cl). The time series infrasound data used in this study are available as a permanent DOI archive (https://doi.org/10.18122/B21B0C) and openly shared via ScholarWorks, Boise State's institutional research repository managed by Albertsons Library and released under a Creative Commons license.

References

Aiuppa, A., Bitetto, M., Francofonte, V., Velasquez, G., Parra, C. B., Giudice, G., et al. (2017). A CO2-gas precursor to the March 2015 Villarrica volcano eruption. *Geochemistry, Geophysics, Geosystems*, *18*, 2120–2132. https://doi.org/10.1002/2017GC006892

Carpenter, M. H., Gottlieb, D., & Abarbanel, S. (1994). Time-stable boundary conditions for finite-difference schemes solving hyperbolic systems: Methodology and application to high-order compact schemes. *Journal of Computational Physics*, *111*(2), 220–236. https://doi.org/10.1006/jcph.1994.1057

Fee, D., Garcés, M., Patrick, M., Chouet, B., Dawson, P., & Swanson, D. (2010). Infrasonic harmonic tremor and degassing bursts from Halema'uma'u crater, Kilauea volcano, Hawaii. *Journal of Geophysical Research*, *115*, B11316. https://doi.org/10.1029/2010JB007642

Fee, D., Haney, M. M., Matoza, R. S., Van Eaton, A. R., Cervelli, P., Schneider, D. J., & Iezzi, A. M. (2017). Volcanic tremor and plume height hysteresis from Pavlof volcano, Alaska. *Science*, *355*(6320), 45–48. https://doi.org/10.1126/science.aah6108

Fee, D., & Matoza, R. S. (2013). An overview of volcano infrasound: From Hawaiian to Plinian, local to global. *Journal of Volcanology and Geothermal Research*, *249*, 123–139. https://doi.org/10.1016/j.jvolgeores.2012.09.002

Goto, A., & Johnson, J. B. (2011). Monotonic infrasound and Helmholtz resonance at Volcan Villarrica (Chile). *Geophysical Research Letters*, *38*, L06301. https://doi.org/10.1029/2011GL046858

Johnson, J. B., Aster, R. C., & Kyle, P. R. (2004). Volcanic eruptions observed with infrasound. *Geophysical Research Letters*, *31*, L14604. https://doi.org/10.1029/2004gl020020

Johnson, J. B., Anderson, J., Marcillo, O., & Arrowsmith, S. (2012). Probing local wind and temperature structure using infrasound from Volcan Villarrica (Chile). *Journal of Geophysical Research*, *117*, D17107. https://doi.org/10.1029/2012JD017694

Johnson, J. B., & Miller, A. J. C. (2014). Application of the monopole source to quantify explosive flux during Vulcanian explosions at Sakurajima volcano (Japan). *Seismological Research Letters*, *85*, 1163–1176. https://doi.org/10.1785/0220140058

Johnson, J. B., & Palma, J. L. (2015). Lahar infrasound associated with Volcán Villarrica's 3 March 2015 eruption. *Geophysical Research Letters*, *42*, 6324–6331. https://doi.org/10.1002/2015GL065024

Johnson, J. B., & Ripepe, M. (2011). Volcano infrasound: A review. *Journal of Volcanology and Geothermal Research*, *206*(3-4), 61–69. https://doi.org/10.1016/j.jvolgeores.2011.06.006

Karlstrom, L., & Dunham, E. M. (2016). Excitation and resonance of acoustic-gravity waves in a column of stratified, bubbly magma. *Journal of Fluid Mechanics*, *797*, 431–470. https://doi.org/10.1017/jfm.2016.257

Kim, K., & Lees, J. M. (2014). Local volcano infrasound and source localization investigated by 3D simulation. *Seismological Research Letters*, *85*(6), 1177–1186. https://doi.org/10.1785/0220140029

Lighthill, M. J. (1978). *Waves in fluids*. New York: Cambridge University Press.

Lyons, J. J., Haney, M. M., Werner, C., Kelly, P., Patrick, M., Kern, C., & Trusdell, F. (2016). Long period seismicity and very long period infrasound driven by shallow magmatic degassing at Mount Pagan, Mariana Islands. *Journal of Geophysical Research: Solid Earth*, *121*, 188–209. https://doi.org/10.1002/2015JB012490

Marcillo, O., Johnson, J. B., & Hart, D. (2012). Implementation, characterization, and evaluation of an inexpensive low-power low-noise infrasound sensor based on a micromachined differential pressure transducer and a mechanical filter. *Journal of Atmospheric and Oceanic Technology*, *29*(9), 1275–1284. https://doi.org/10.1175/JTECH-D-11-00101.1

Matoza, R. S., Fee, D., Neilsen, T. B., Gee, K. L., & Ogden, D. E. (2013). Aeroacoustics of volcanic jets: Acoustic power estimation and jet velocity dependence. *Journal of Geophysical Research: Solid Earth*, *118*, 6269–6284. https://doi.org/10.1002/2013JB010303

Morrissey, M. M., & Chouet, B. A. (1997). Burst conditions of explosive volcanic eruptions recorded on microbarographs. *Science*, *275*(5304), 1290–1293. https://doi.org/10.1126/science.275.5304.1290

Moussallam, Y., Bani, P., Curtis, A., Barnie, T., Moussallam, M., Peters, N., et al. (2016). Sustaining persistent lava lakes: Observations from high-resolution gas measurements at Villarrica volcano, Chile. *Earth and Planetary Science Letters*, *454*, 237–247. https://doi.org/10.1016/j.epsl.2016.09.012

Newhall, C. G., & Self, S. (1982). The volcanic explosivity index (VEI) an estimate of explosive magnitude for historical volcanism. *Journal of Geophysical Research*, *87*, 1231–1238. https://doi.org/10.1029/JC087iC02p01231

Olson, H. F. (1957). *Acoustical engineering* (pp. 88–123). Princeton, NJ: Van Nostrand-Reinhold.

Palma, J. L., Calder, E. S., Basualto, D., Blake, S., & Rothery, D. A. (2008). Correlations between SO2 flux, seismicity, and outgassing activity at the open vent of Villarrica volcano, Chile. *Journal of Geophysical Research*, *113*, B10201. https://doi.org/10.1029/2008JB005577

Richardson, J. P., Waite, G. P., & Palma, J. L. (2014). Varying seismic-acoustic properties of the fluctuating lava lake at Villarrica volcano, Chile. *Journal of Geophysical Research: Solid Earth*, *119*, 5560–5573. https://doi.org/10.1002/2014JB011002

Ripepe, M., Marchetti, E., Bonadonna, C., Harris, A. J. L., Pioli, L., & Uliveri, G. (2010). Monochromatic infrasonic tremor driven by persistent degassing and convection at Villarrica volcano, Chile. *Geophysical Research Letters*, *37*, L15303. https://doi.org/10.1029/2010GL043516

Rossing, T. D., & Fletcher, N. H. (2004). *Principles of vibration and sound* (2nd ed., pp. 157–207). New York: Springer.

Spina, L., Cannata, A., Privitera, E., Vergniolle, S., Ferlito, C., Gresta, S., et al. (2014). Insights into Mt. Etna's shallow plumbing system from the analysis of infrasound signals, August 2007–December 2009. *Pure and Applied Geophysics*, *172*(2), 473–490. https://doi.org/10.1007/s00024-014-0884-x

Svard, M., & Nordstrom, J. (2014). Review of summation-by-parts schemes for initial-boundary-value problems. *Journal of Computational Physics*, *268*, 17–38. https://doi.org/10.1016/j.jcp.2014.02.031

Van Daele, M., Moernaut, J., Silversmit, G., Schmidt, S., Fontijn, K., Heirman, K., et al. (2014). The 600 yr eruptive history of Villarrica volcano (Chile) revealed by annually laminated lake sediments. *Geological Society of America Bulletin*, *126*(3-4), 481–498. https://doi.org/10.1130/B30798.1

Woulff, G., & McGetchin, T. R. (1976). Acoustic noise from volcanoes—Theory and experiment. *Geophysical Journal of the Royal Astronomical Society*, *45*(3), 601–616. https://doi.org/10.1111/j.1365-246X.1976.tb06913

Yamasato, H. (1997). Quantitative analysis of pyroclastic flows using infrasonic and seismic data at Unzen volcano, Japan. *Journal of Physics of the Earth*, *45*(6), 397–416. https://doi.org/10.4294/jpe1952.45.397